Photon-recycling by Energy Transfer in Piezochemically Synthesized and Close-packed Methyl Ammonium Lead Halide Perovskites

Sushant Ghimire, Kiyonori Takahashi, Yuta Takano, Takayoshi Nakamura, Vasudevanpillai Biju*

Research Institute for Electronic Science and Graduate School of Environmental Science, Hokkaido University N20, W10, Sapporo, Hokkaido 001-0020, JAPAN

*Address correspondence to: biju@es.hokudai.ac.jp

Abstract

Photon-recycling by multiple reabsorption-emission is responsible for the long-range energy transport in large crystals and thick films of lead halide perovskites, resulting in red-shifted and delayed emission. Apart from such a radiative process, nonradiative energy transfer influences photon recycling in perovskites with close-packed donor-acceptor type states. In this study, we report the role of nonradiative energy transfer on photon-recycling in piezochemically synthesized and close-packed pure and mixed halide methylammonium lead perovskites. Here the pressure applied to precursors of perovskites helps us to synthesize and close-pack perovskite crystallites into pellets. Nonetheless, interestingly, we find that the applied pressure redistributes the emission maxima or band-gap of these perovskites. The temporally- and spectrally- resolved photoluminescence from the mixed halide sample unveils nonradiative energy transfer from a higher (bromide) to a lower (iodide) band-gap domains, where the rate of relaxation of the bromide domain is higher than that of pure bromide perovskite. These results help us to confirm the role of nonradiative energy transfer on photon-recycling in perovskites.

1. Introduction

The solution processability, brilliant luminescence, and high carrier mobility make lead halide perovskites attractive for lighting[1-7] and light-harvesting applications.[8-11] In this frame, record-breaking long-range carrier diffusion and high-power conversion efficiencies are demonstrated using high-quality crystals and close-packed films of halide perovskites.[1,2,4,5,10-13] However, when the material thickness becomes considerably large, reabsorption of emitted photons by the sample itself takes place.[14] Owing to the high internal quantum yield and a large absorption-emission spectral overlap in a perovskite film or crystal, the emitted photons re-excite the sample, resulting in re-emission. Such a phenomenon of multiple self-absorption and re-emission is called photon recycling which enables photons to cascade through a perovskite sample and as the result, the low energy photons are emitted at locations away from the point of photoexcitation.[15-22]

In lead halide perovskites, photon-recycling was first demonstrated in methylammonium lead iodide ($MAPbI_3$) single crystals by Yamada *et al.*[15] which was by time-resolved PL measurements under one- and two-photon excitations. Later, the process of photon-recycling was also shown in the thick crystals of methylammonium lead bromide ($MAPbBr_3$) and methylammonium lead chloride ($MAPbCl_3$) by Kanemitsu and coworkers.[16,20] Similarly, Friend and coworkers[17] have shown an increase in the excited-state population in a $MAPbI_3$ perovskite solar cell, which is due to photon-recycling, allowing for high open-circuit voltages. They emphasized that the long-range energy transport is not only limited to a carrier diffusion length but also occurs through repeated recycling between photons and electron-hole pairs. On contrary, Fang *et al.*[23] have reported very small photon-recycling efficiencies (<0.5%) in $MAPbBr_3$ and $MAPbI_3$ perovskite microcrystals, underscoring the intrinsically long carrier recombination lifetime instead of photon propagation mediated by photon-recycling. However,

they did not exclude the possibility of photon-recycling in polycrystalline films of perovskites. Recently, Gan *et al*.[22] have confirmed photon-recycling as the dominant process responsible for the red-shifted and delayed emission in two-dimensional lead halide perovskites, where the interplane carrier migration is highly suppressed by the multi-quantum-well structure. They also revealed that, in a three-dimensional bulk $MAPbBr_3$ perovskite single crystal, the carrier migration contributes to the energy transport process; however, the contribution is negligibly small at a distance beyond the diffusion length. These studies show that photon-recycling and charge-carrier migration are two important phenomena which influence PL and carrier dynamics in lead halide perovskites. Besides, a nonradiative energy transfer through the distributed energy states among different crystalline domains in close-packed perovskite structures should also be considered. Some studies have shown energy transfer among lead halide perovskite nanocrystals of different sizes or compositions which exhibit different band-gaps in the film,[24] aggregate,[25] or colloidal solution state.[26] However, the role of nonradiative energy transfer on photon-recycling in close-packed perovskite structures is yet to be clarified. It is obvious that the efficiency of energy transfer in such structures should depend upon the degree of close-packing and the composition of the crystallites. In this regard, the preparation, processing and close-packing of perovskites become important.

So far, close-packed lead halide perovskites are realized in the form of single crystals,[1,2,4,5] nanocrystals self-assembly,[10,11] films,[12,13,17,24] and clusters,[25,27] where the samples are synthesized by the wet-chemical routes. The solvent plays essential roles on the morphology, growth, and stability of the perovskite structure. Though wet-chemistry renders high-quality perovskite films and crystals, dry solvents and inert atmosphere are essential since moisture and oxygen affect the optical properties of perovskites.[28,29] Mechanochemical synthesis is a solvent-free method for the synthesis of perovskites, which involves direct grinding or ball-milling of precursors.[30-33] While the mechanical force is a major driving

parameter in the solid-state reaction among perovskite precursors, pressure is another major thermodynamic parameter that influences the formation and stability of perovskite lattices.[34] Although studies on the effect of pressure on the electro-optical properties and the crystal structures of perovskites are carried out,[35-37] piezochemical synthesis is an overlooked subject in chemistry. In this work, the term 'piezochemistry' is defined as the chemical change, reaction or modification resulting from the application of mechanical stress or pressure. Furthermore, in close-packed perovskites, energy transfer through the distributed states is significant, the role of which on photon-recycling is yet to be rationalized. Here, we report efficient nonradiative energy transfer among piezochemically synthesized and close-packed lead halide perovskite crystallites. In the study, we introduce piezochemical synthesis to prepare close-packed pristine methylammonium lead halide [$MAPbX_3$ (X=Cl, Br, I)] perovskites, and the method is further extended to mixed bromide-iodide ($MAPbBr_{3-x}I_x$) heterojunction perovskites.

2. Experimental Methods

For the piezochemical synthesis of lead halide perovskites in the form of pellets, we used the following precursors as received. Methylamine hydrochloride (MACl, TCI, >98.0%), methylamine hydrobromide (MABr, TCI, >98.0%), methylamine hydroiodide (MAI, TCI, >98.0%), lead (II) chloride ($PbCl_2$, Sigma-Aldrich, 98%), lead (II) bromide ($PbBr_2$, Sigma-Aldrich, ≥98%), and lead (II) iodide (PbI_2, Sigma-Aldrich, 99%).

2.1 Piezochemical synthesis of $MAPbX_3$ (X=Cl, Br, I) and mixed bromide-iodide ($MAPbBr_{3-x}I_x$) heterojunction perovskites

In typical synthesis of a $MAPbX_3$ perovskite, PbX_2 (1.35 mmol) and MAX (1.25 mmol) were crushed separately into fine powder, which was by using a hand mortar, and thoroughly mixed by flipping the vial up and down. The precursor mixture was filled inside a silicon

chamber (20 mm in diameter) placed on a metal plate, which was followed by applying pressure using a brass rod tip in a hydraulic jack. After 30 min, the pressure was released to obtain a disk-shaped perovskite pellet. We employed different pressures (1.2 GPa, 2.4 GPa, 3.6 GPa, 4.8 GPa, or 6 GPa) and identified the optimum pressure for the synthesis. The amounts of chemicals used during the reactions are tabulated in Table 1.

Table 1. The amount of chemicals used in the piezochemical synthesis of $MAPbX_3$ (X=Cl, Br, I) and mixed bromide-iodide ($MAPbBr_{3-x}I_x$) heterojunction perovskite pellets.

S.N.	Samples	Precursor salts	Amount mg (mmol)
1.	$MAPbCl_3$	$PbCl_2$	375 (1.35)
		MACl	85 (1.25)
2.	$MAPbBr_3$	$PbBr_2$	500 (1.35)
		MABr	140 (1.25)
3.	$MAPbI_3$	PbI_2	622 (1.35)
		MAI	199 (1.25)
4.	$MAPbBr_{3-x}I_x$	$PbBr_2$	275 (0.75)
		MABr	84 (0.75)
		PbI_2	115 (0.25)

The piezochemical synthesis method was extended to obtain a mixed bromide-iodide ($MAPbBr_{3-x}I_x$) heterojunction perovskite. In typical synthesis, we thoroughly mixed the precursors $PbBr_2$ (0.75 mmol), CH_3NH_3Br (0.75 mmol) and PbI_2 (0.25 mmol) [for the calculated amounts of precursors, see Table 1]. To this precursor mixture, a pressure of 2.4 GPa was applied to obtain a mixed bromide-iodide heterojunction perovskite pellet.

2.2 Characterization of perovskite samples

Optical characterization of perovskite samples was carried out by measuring the reflectance spectra using a UV-Vis spectrophotometer (Evolution 220, Thermo Fischer

Scientific). Tauc plots were constructed from the reflectance spectra to estimate the band-gaps of the samples.

To characterize the crystalline phase of perovskites, powder X-ray diffraction (XRD) measurements were carried out in an X-ray diffractometer (RINT 2200, Rigaku), and the obtained XRD patterns were compared with the reference spectra in the literature and confirmed the perovskite structures. The samples for XRD measurements were prepared by crushing the perovskite pellets into fine powder and drying it under vacuum for 5 h. For each measurement, about 30 mg of powdered perovskite sample was used.

2.3 Time-resolved PL spectroscopy

Time-resolved PL spectroscopy was used to study the PL properties of perovskite pellets and the mechanism of energy transfer in them. The excitation light for time-resolved PL measurements was 400 nm femtosecond pulses (150 fs) generated from the second harmonic generator (SHG) crystal of an Optical Parametric Amplifier (Coherent OPA 9400). The OPA was pumped at 200 KHz with the amplified femtosecond pulses from a Regenerative Amplifier (Coherent RegA 9000), which was seeded by the 800 nm pulses from a mode-locked oscillator (Coherent Mira 900). Spectrally- and temporally- resolved photons were recorded using an assembly of a polychromator (model 250IS, Chromex) and a photon-counting streak-camera (model C4334, Hamamatsu). A schematic illustration of the optical setup for the time-resolved PL micro-spectroscopy is shown in Figure 1.

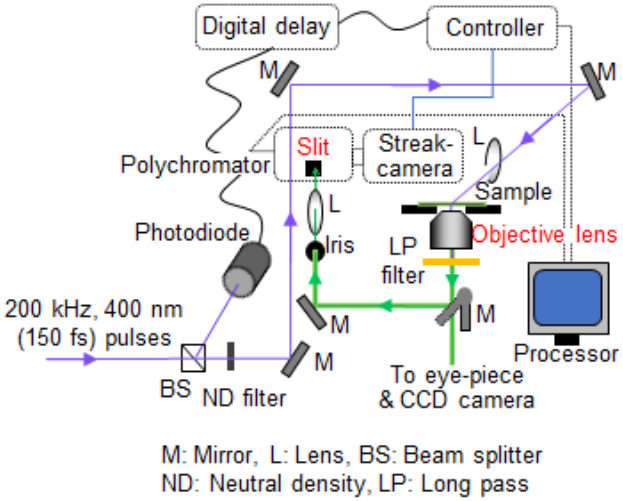

Figure 1. Optical setup for the time-resolved PL micro-spectroscopy.

The PL signals from the perovskite samples deposited on a glass substrate in an inverted microscope (Olympus IX70) were passed through an objective lens (40×, NA 0.60, Olympus UmPlan), filtered through a 440 nm long-pass filter, and focused using a lens at the entrance slit of the polychromator (Figure 1). The signals were detected using the streak-camera. For the power-dependent PL studies, the laser power was varied by using neutral density filters.

3. Results and Discussion

The scheme for the piezochemical synthesis of lead halide perovskites is shown in Figure 2a. Disk-shaped perovskite pellets of thickness ca 1 mm and diameter 20 mm are obtained by applying a hydraulic pressure of 2.4 GPa to a solid and homogenous mixture of precursor salts for 30 minutes. Figure 2b shows the photographs of $MAPbCl_3$, $MAPbBr_3$, and $MAPbI_3$ perovskite pellets which were prepared by the piezochemical synthesis. During the synthesis, the hydraulic pressure acts as a driving force for the chemical reaction of perovskite precursors. While the earlier reports demonstrate the effect of applied pressure on

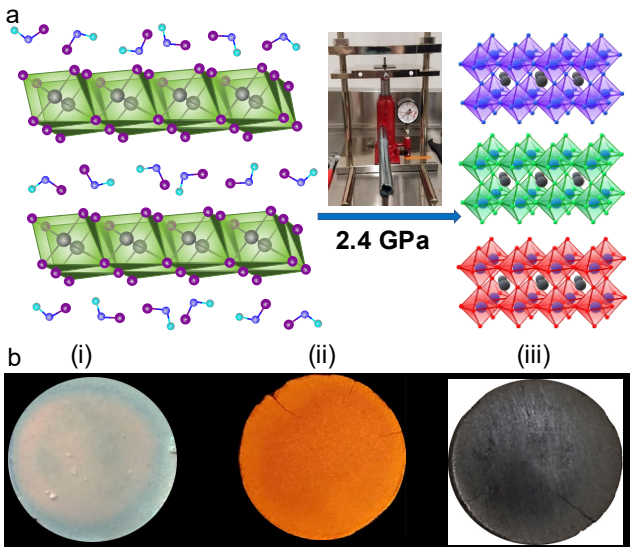

Figure 2. Piezochemical synthesis and close-packing of $MAPbX_3$ (X=Cl, Br, I) perovskites. a) Scheme of synthesis and b) photographs of (i) $MAPbCl_3$, (ii) $MAPbBr_3$, and (iii) $MAPbI_3$ perovskite pellets.

the PL properties of perovskites,[35-37] to our knowledge, this is the first time we are demonstrating the piezochemical synthesis of lead halide perovskites. We hypothesize that in the piezochemical synthesis, the applied pressure helps to transform the edge-sharing orthorhombic PbX_2 chains into corner-sharing PbX_6 octahedra, which is assisted by the pressure-induced deformation of MAX, leading to the transfer of halide ion to form the octahedra. In parallel to the reorganization of halide ion and PbX_2 into the corner-sharing octahedra, MA^+ is pushed into the space between the octahedra to form stable perovskite structure.

To characterize the crystal structure of perovskites, we carried out X-ray diffraction (XRD, Figure 3a) analyses. The XRD pattern of $MAPbCl_3$ reveals cubic crystalline phase, consistent with the phase of crystals prepared by wet chemical methods.[7,38] In the case of $MAPbBr_3$, the XRD data reveal a mixture of cubic and orthorhombic phases. The Bragg's diffraction peaks of $MAPbBr_3$ at 14.90°, 21.18°, 30.13°, 33.83°, 37.15°, 43.14° and 45.93°, respectively

correspond to100, 110, 200, 210, 211, 220 and 300 crystal planes of the cubic phase.[39,40] The existence of orthorhombic phase is confirmed by the splitting of a diffraction peak at 30.13° (200 crystal plane) and the appearance of a new peak at 30.56° (121 crystal plane).[39,41] $MAPbI_3$ perovskite shows tetragonal crystalline phase with characteristic diffraction peaks at 13.99°, 19.86°, 23.46°, 24.48°, 28.36°, 31.79°, 34.29°, 34.95°, 40.56°, and 43.08°.[42] The corresponding crystal planes are respectively 110 or 002, 112, 211, 202, 004 or 200, 114 or 222, 024, 312, 224 or 040, and 314 or 330.

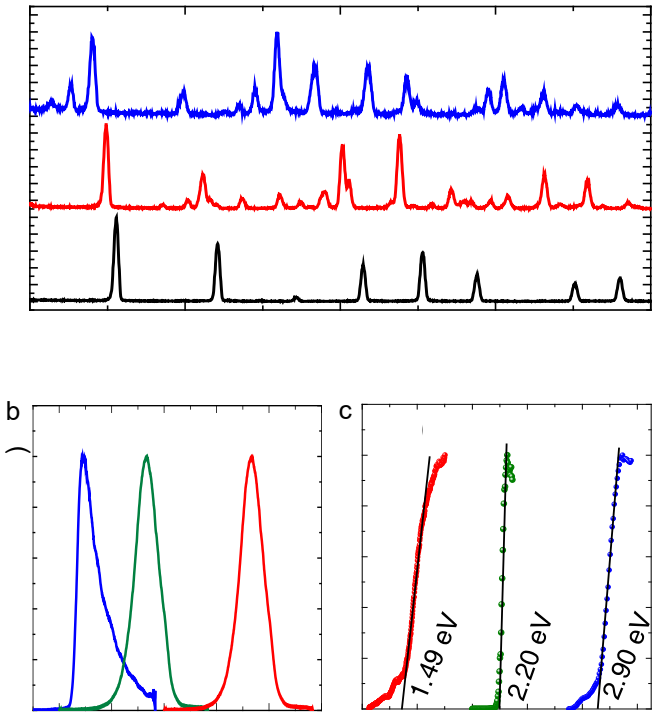

Figure 3. Characterization of $MAPbX_3$ (X=Cl, Br, I) perovskites. a) Powder XRD pattern, b) PL spectra, and c) the Tauc plots of (i) $MAPbCl_3$, (ii) $MAPbBr_3$, and (iii) $MAPbI_3$ perovskite pellets.

We investigate the optical properties of $MAPbX_3$ perovskite pellets using PL and UV-Vis reflectance spectroscopic techniques. The PL spectra (Figure 3b) show characteristic blue (ca 450 nm), green (ca 560 nm) and near infrared (NIR, ca 760 nm) emission peaks of $MAPbCl_3$,

$MAPbBr_3$ and $MAPbI_3$ perovskites, respectively. The variation of emission wavelength is correlated with the change in optical band-gap of the perovskites. We obtained the band-gaps of $MAPbX_3$ perovskites from the Tauc plots (Figure 3c). The band-gap values for $MAPbCl_3$, $MAPbBr_3$, and $MAPbI_3$ are 2.90, 2.20, and 1.49 eV, respectively. The decrease in band-gap in the order Eg($MAPbCl_3$) > Eg($MAPbBr_3$) > Eg($MAPbI_3$) is consistent with the PL red-shift, which can be assigned to the enhanced spin-orbital coupling (SOC) by changing the halide composition from Cl to Br to I.[43-46] Apart from the halogen-induced red-shift, the PL maxima of these pellets are further red-shifted when compared to the nanocrystal counterparts.[3] Also, the pellets show low PL intensity. These red-shifted and low intensity PL bands suggests considerable reabsorption of emitted photons in such thick pellets, which is similar to the photon-recycling process observed in thick films and large single crystals of perovskites.[14-22] Although the PL intensity from the thick pellets was extremely low, which is due to the repeated nonradiative relaxation throughout the repeated reabsorption and nonradiative energy transfer processes, isolated crystallites in the pellets were brilliantly luminescent (Supporting Information, Figure S1). Further, the Tauc plots of $MAPbX_3$ perovskites in Figure 3c show low energy tails, which is attributed to the heterogeneity of the samples induced by the applied pressure. We firmly believe that such heterogeneity in the structure or packing of the perovskite crystallites introduces distributed energy states or bands in the pellets. Also, we do not rule out the scattering of excitation light by crystallites of perovskites and unreacted precursors.

To rationalize the mechanism of photon-recycling through the distributed bands, we prepared close-packed mixed bromide-iodide ($MAPbBr_{3-x}I_x$) heterojunction perovskites by the piezochemical synthesis. Based on the band-gaps, we consider the bromide-rich domain to be the energy donor and the iodide-rich domain to be the energy acceptor. To evaluate energy transfer from the bromide- to iodide- rich domains, we recorded time-resolved PL at

the heterojunction. Figure 4a shows the microscopic PL image of a heterojunction perovskite pellet, and the PL spectra recorded at the bromide- and iodide-rich domains are shown in Figure 4b. As seen in Figure 4a, the pellet has bromide-rich (green), iodide-rich (NIR), and mixed bromide-iodide (red) domains. The distinct bromide- and iodide- rich domains help us to discuss photon-recycling in terms of energy transfer. As we move from the bromide- to iodide- rich domains, the intensity of the band ca 550 nm becomes smaller and smaller, which is accompanied by higher and higher intensity emission ca 750 nm (Figure 4b). Nonetheless, difference in the ratio of composition of bromide and iodide across different heterojunctions cannot be ruled out based on the PL intensity variations in these regions.

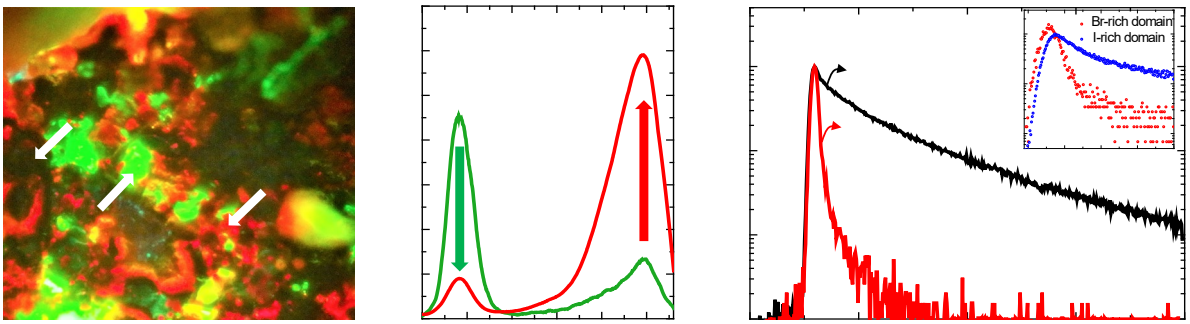

Figure 4. Photon-recycling through nonradiative energy transfer in a mixed bromide-iodide ($MAPbBr_{3-x}I_x$) heterojunction perovskite. a) PL image of a $MAPbBr_{3-x}I_x$ perovskite pellet. The image size is 100 µm x 100 µm. b) PL spectra of a $MAPbBr_{3-x}I_x$ perovskite pellet collected from (green) bromide-rich and (red) iodide-rich domains. c) PL decay profiles of (i) pristine $MAPbBr_3$ and (ii) a bromide-rich domain in a mixed bromide-iodide ($MAPbBr_{3-x}I_x$) perovskite pellet. The two decays were collected in the 500-575 nm region. Inset: PL decay profiles of a bromide-rich and an iodide-rich domain.

To further confirm energy transfer from bromide- to iodide- rich domains, we examined the PL decay profiles of a donor at the heterojunction and compared it with that of pristine $MAPbBr_3$ (Figure 4c). Interestingly, the PL lifetime of a green-emitting domain is much

shorter (ca 1.77±0.33 ns) than that of pristine $MAPbBr_3$ (ca 15.56±3.89 ns), indicating that the iodide-rich domain plays an important role on the deactivation of photoexcited bromide-rich domain. Photon-recycling by reabsorption of emitted photon cannot account for the decreased PL lifetime of the donor. Based on these PL lifetime values, an efficient nonradiative energy transfer from the bromide- to iodide- rich domains is apparent. The energy transfer from a wide band-gap bromide-rich domain to a narrow band-gap iodide-rich domain is further supported by the PL rise shown in the inset of Figure 4c. Precise evaluation of the PL rise time is hindered by the emission from directly-excited iodide-rich domain. Here the PL decay becomes faster with increase in intensity of the excitation light, which is due to an increase in the amplitude of intrinsic emission from the iodide-rich domain. The excitation laser intensity-dependent PL decay profiles of bromide- and iodide- rich domains are shown in the supporting information (Figure S2). On the other hand, the mixed bromide-iodide domain is not clearly observed in the PL spectra (Figure 4b) which suggests that the mixed halide domains act as both the acceptor for the bromide-rich domain and the efficient donor for the iodide-rich domain. In other words, the mixed halide domain mediates efficient energy transfer to the acceptor.

We estimated the rate of nonradiative energy transfer in mixed bromide-iodide ($MAPbBr_{3-x}I_x$) heterojunction perovskites by comparing the PL lifetimes of pristine $MAPbBr_3$ perovskite with the bromide-rich domain of the heterojunction using equations 1 and 2 as follows:

$$\tau_0 = \frac{1}{k_r + k_{nr}} \tag{1}$$

$$\tau = \frac{1}{k_{\mathrm{r}} + k_{\mathrm{nr}} + k_{\mathrm{et}}} \tag{2}$$

where, τ_0 and τ are the PL lifetimes of a pristine $MAPbBr_3$ perovskite pellet and green-emitting (bromide-rich) domain at the heterojunction, respectively; k_r and k_{nr} are the rates of radiative and nonradiative relaxations, respectively; and k_{et} is the rate of energy transfer.

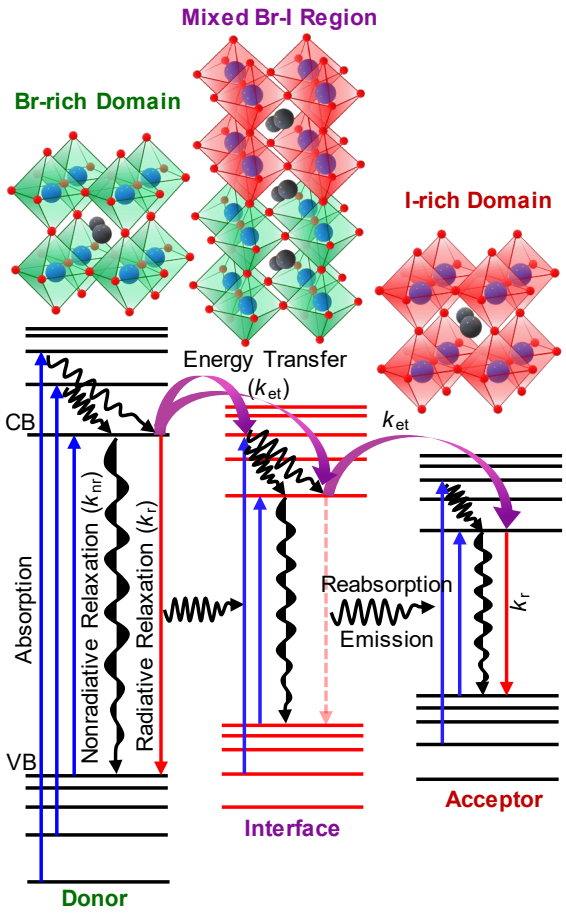

Figure 5. A scheme of photon-recycling and energy transfer in a mixed bromide-iodide heterojunction perovskite pellet.

From τ_0 (15.56 ns) and τ (1.77 ns), the rate of energy transfer is estimated at $5x10^8$ s^{-1} which is one order of magnitude higher than the rate of carrier recombination (radiative and nonradiative) in pristine $MAPbBr_3$ ($1/\tau_0=6x10^7$ s^{-1}). Here, the reabsorption of emitted photons does not add any additional path for the deactivation of the excited state in a mixed bromide-iodide heterojunction perovskite. Thus, a considerably decreased τ and a high k_{et} value show

that nonradiative energy transfer plays a key role on photon-recycling process in perovskites. Although k_{et} is discussed in terms of energy transfer, the contribution of interdomain charge migration or electron transfer is not ruled out.

Despite the fact that the emitted photons contribute to photon-recycling, the above results clearly show that the role of nonradiative energy transfer on photon-recycling should be considered alongside. Various radiative and nonradiative processes involved in photon-recycling are summarized schematically in Figure 5. The valance and conduction bands of the bromide-rich donor and the iodide-rich acceptor are shown to the left and right parts of the scheme, respectively, and the energy bands formed due to halogen exchange or mixed-halide formation at the interface are shown in between. Here, the band-gap of a mixed halide domain is intermediate between the bromide-rich donor and iodide-rich acceptor. During photoexcitation, the photons absorbed by all the three domains across the heterojunction undergo various radiative and nonradiative relaxations. In addition, some of the emitted photons are reabsorbed and emitted again. Nevertheless, when nonradiative energy transfer overcomes the inter-band radiative relaxation, the excited state of the donor is depopulated by efficiently transferring the energy to the mixed halide or iodide domain. As discussed previously (in Figure 4), the mixed-halide region helps to funnel the energy efficiently from bromide- to iodide- rich domains, but without undergoing radiative relaxation.

The efficiency of nonradiative energy transfer depends upon the degree of close-packing. We estimate the efficiency of nonradiative energy transfer in the heterojunction perovskite pellet synthesized at a pressure of 2.4 GPa, which is using the equation 3,

$$\eta=1-\tau_{DA}/\tau_{D} \quad (3)$$

where, η is the efficiency of energy transfer, τ_{DA} is the PL lifetime of donor (Br-rich domain) in the presence of acceptor (I-rich domain) and τ_{D} is the PL lifetime of donor in the absence

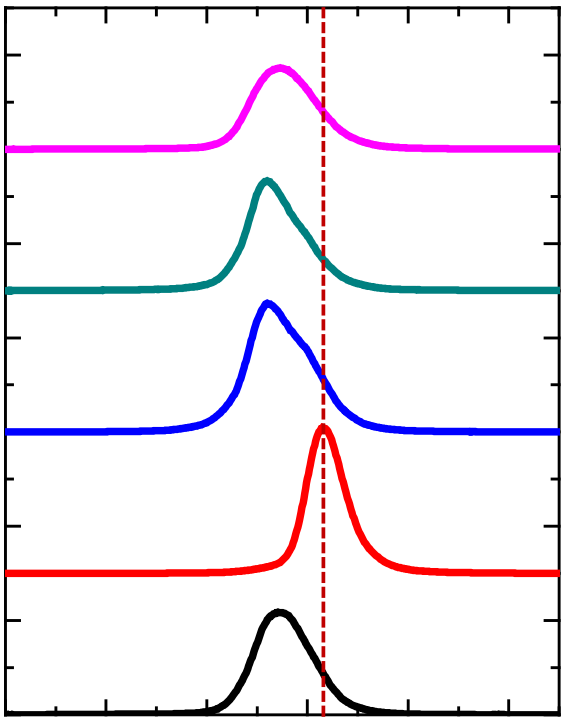

Figure 6. The pressure-dependent PL spectra of $MAPbBr_3$ perovskite pellets.

of acceptor (pristine $MAPbBr_3$ pellet). For τ_{DA}=1.77 ns and τ_D=15 ns, we estimate η at 0.88, which is quite high and supports the the role of efficient nonradiative energy transfer in photon-recycling in heterojunction perovskites. Besides, we also synthesized $MAPbBr_3$ perovskite pellets by applying *in-situ* pressures of 1.2, 3.6, 4.8 and 6.0 GPa, the PL spectra of which, along with that synthesized at 2.4 GPa, are given in Figure 6. Initially, a red-shift of ca 90 meV in the PL maximum with spectral narrowing is observed, which was upon increasing the pressure from 1.2 (full width at half maximum, FWHM=34 nm) to 2.4 (FWHM=23 nm) GPa. These changes are attributed to the Pb-X-Pb bond-length compression. Beyond 2.4 GPa, a blue-shift of ca 120 meV in the PL maximum and an increase in spectral broadening (FWHM=34 nm) are detected up to 4.8 GPa. This is ascribed to the octahedral tilt, which is the deviation of Pb-X-Pb bond-angle from the ideal value of 180° in the cubic cell lattice. At the maximum applied pressure of 6.0 GPa, further spectral broadening (FWHM=38 nm) and red-shift of ca 30 meV in the PL maximum are observed, suggesting the disordering of

organic cation and amorphization of the perovskite lattice. The pressure-dependence of PL spectra in perovskite pellets is due to the enhancement and weakening of SOC as the result of compression of Pb-X bond and shrinkage of Pb-X-Pb bond-angle, respectively.[35-37] Here, a huge shift of (ca 120 meV) PL spectra towards higher energy region in the pressure range of 2.4 to 4.8 GPa suggests that the pressure has affected the octahedral tilting of the perovskite lattice, which alters the band-gap and PL maximum through the weakening of SOC. In closed-packed perovskite crystals with closely-spaced bandgaps, such a shift in PL influences the spectral overlap integral and the efficiency of energy transfer.

In summary, by the piezochemical synthesis and close-packing of lead halide perovskites, we demonstrate the role of nonradiative energy transfer on photon-recycling in them. We synthesized pristine $MAPbX_3$ (X=Cl, Br, I) and mixed bromide-iodide ($MAPbBr_{3-x}I_x$) heterojunction perovskite pellets by applying a hydraulic pressure to their powdered precursors. We analyzed the role of energy transfer in photon-recycling in these perovskite samples. From the fast deactivation of the excited state of the donor (bromide-rich domain) and the associated delayed emission from the acceptor (iodide-rich domain) across the heterojunction, we confirm the role of nonradiative energy transfer on photon-recycling in these systems. Our studies suggest that not only repeated absorption and emission but also the nonradiative energy transfer among the distributed energy states contributes significantly to the photon-recycling process in thick, close-packed perovskites.

Keywords: Piezochemistry, heterojunction perovskites • photon-recycling • energy-transfer • solid-state synthesis

AUTHOR INFORMATION

Corresponding Author

*biju@es.hokudai.ac.jp

AUTHOR CONTRIBUTIONS

V. B. conceived the idea, S. G. synthesized perovskites and conducted optical studies, S. G. prepared the manuscript draft, and S. G., Y. T. and V. B. finalized the manuscript. S. G., K. T. and T. N. performed XRD experiments. All authors assisted in discussion and data analysis.

Notes

The authors declare no competing financial interest.

ACKNOWLEDGMENTS

This work was carried out under the support of MEXT JSPS Grant-in-Aid for Scientific Research B (19H02550) and JSPS Grant-in-Aid for Specially Promoted Research (18H05205) It is also supported by the JSPS Dynamic Alliance for Open Innovation Bridging Human, Environment and Materials. S. G. acknowledges a MEXT Scholarship.

References

(1) Shi, D.; Adinolfi, V.; Comin, R.; Yuan, M.; Alarousu, E.; Buin, A.; Chen, Y.; Hoogland, S.; Rothenberger, A.; Katsiev, K.; Losovyj, Y.; Zhang, X.; Dowben, P. A.; Mohammed, O. F.; Sargent, E. H.; Bakr, O. M. Low Trap-State Density and Long Carrier Diffusion in OrganoLead Trihalide Perovskite Single Crystals. *Science* **2015**, *347*, 519-522.

(2) Dong, Q.; Fang, Y.; Shao, Y.; Mulligan, P.; Qiu, J.; Cao, L.; Huang, J. Electron-Hole Diffusion Lengths > 175 μm in Solution-Grown $CH_3NH_3PbI_3$ Single Crystals. *Science* **2015**, *347*, 967-970.

(3) Zhang, F.; Zhong, H.; Chen, C.; Wu, X.; Hu, X.; Huang, H.; Han, J.; Zou, B.; Dong, Y. Brightly Luminescent and Color-Tunable Colloidal $CH_3NH_3PbX_3$ (X = Br, I, Cl) Quantum Dots: Potential Alternatives for Display Technology. *ACS Nano* **2015**, *9*, 4533-4542.

(4) Zhumekenov, A. A.; Saidaminov, M. I.; Haque, M. A.; Alarousu, E.; Sarmah, S. P.; Murali, B.; Dursun, I.; Miao, X. H.; Abdelhady, A. L.; Wu, T.; Mohammed, O. F.;

Bakr, O. M. Formamidinium Lead Halide Perovskite Crystals with Unprecedented Long Carrier Dynamics and Diffusion Length. *ACS Energy Lett.* **2016**, *1*, 32-37.

(5) Bi, Y.; Hutter, E. M.; Fang, Y.; Dong, Q.; Huang, J.; Savenije, T. J. Charge Carrier Lifetimes Exceeding 15 μs in Methylammonium Lead Iodide Single Crystals. *J. Phys. Chem. Lett.* **2016**, *7*, 923-928.

(6) Levchuk, I.; Osvet, A.; Tang, X.; Brandl, M.; Perea, J. D.; Hoegl, F.; Matt, G. J.; Hock, R.; Batentschuk, M.; Brabec, C. J. Brightly Luminescent and Color-Tunable Formamidinium Lead Halide Perovskite FAPbX3 (X = Cl, Br, I) Colloidal Nanocrystals. *Nano Lett.* **2017**, *17*, 2765-2770.

(7) Maculan, G.; Sheikh, A. D.; Abdelhady, A. L.; Saidaminov, M. I.; Haque, M. A.; Murali, B.; Alarousu, E.; Mohammed, O. F.; Wu, T.; Bakr, O. M. $CH_3NH_3PbCl_3$ Single Crystals: Inverse Temperature Crystallization and Visible-Blind UV-Photodetector. *J. Phys. Chem. Lett.* **2015**, *6*, 3781-3786.

(8) Xing, G.; Mathews, N.; Lim, S. S.; Yantara, N.; Liu, X.; Sabba, D.; Grätzel, M.; Mhaisalkar, S.; Sum, T. C. Low-Temperature Solution-Processed Wavelength-Tunable Perovskites for Lasing. *Nat. Mater.* **2014**, *13*, 476-480.

(9) Sadhanala, A.; Ahmad, S.; Zhao, B.; Giesbrecht, N.; Pearce, P. M.; Deschler, F.; Hoye, R. L. Z.; Gödel, K. C.; Bein, T.; Docampo, P.; Dutton, S. E.; De Volder, M. F. L.; Friend, R. H. Blue-Green Color Tunable Solution Processable Organolead Chloride–Bromide Mixed Halide Perovskites for Optoelectronic Applications. *Nano Lett.* **2015**, *15*, 6095-6101.

(10) Nair, V. C.; Muthu, C.; Rogach, A. L.; Kohara, R.; Biju, V. Channeling Exciton Migration into Electron Transfer in Formamidinium Lead Bromide Perovskite Nanocrystal/Fullerene Composites. *Angew. Chem. Int. Ed.* **2017**, *56*, 1214-1218.

(11) Ghimire, S.; Chouhan, L.; Takano, Y.; Takahashi, K.; Nakamura, T.; Yuyama, K.; Biju, V. Amplified and Multicolor Emission from Films and Interfacial Layers of Lead Halide Perovskite Nanocrystals. *ACS Energy Lett.* **2019**, *4*, 133-141.

(12) Saba, M.; Cadelano, M.; Marongiu, D.; Chen, F.; Sarritzu, V.; Sestu, N.; Figus, C.; Aresti, M.; Piras, R.; Geddo Lehmann, A.; Cannas, C.; Musinu, A.; Quochi, F.; Mura, A.; Bongiovanni, G. Correlated Electron−Hole Plasma in Organometal Perovskites. *Nat. Commun.* **2014**, *5*, 5049.

(13) deQuilettes, D. W.; Vorpahl, S. M.; Stranks, S. D.; Nagaoka, H.; Eperon, G. E.; Ziffer, M. E.; Snaith, H. J.; Ginger, D. S. Impact of Microstructure on Local Carrier Lifetime in Perovskite Solar Cells. *Science* **2015**, *348*, 683-686.

(14) Diab, H.; Arnold, C.; Ledée, F.; Trippe-Allard, G.; Delport, G.; Vilar, C.; Bretenaker, F.; Barjon, J.; Lauret, J.-S.; Deleporte, E.; Garrot, D. Impact of Reabsorption on the Emission Spectra and Recombination Dynamics of Hybrid Perovskite Single Crystals. *J. Phys. Chem. Lett.* **2017**, *8*, 2977-2983.

(15) Yamada, Y.; Yamada, T.; Phuong, L. Q.; Maruyama, N.; Nishimura, H.; Wakamiya, A.; Murata, Y.; Kanemitsu, Y. Dynamic Optical Properties of $CH_3NH_3PbI_3$ Single Crystals as Revealed by One- and Two-Photon Excited Photoluminescence Measurements. *J. Am. Chem. Soc.* **2015**, *137*, 10456-10459.

(16) Yamada, T.; Yamada, Y.; Nishimura, H.; Nakaike, Y.; Wakamiya, A.; Murata, Y.; Kanemitsu, Y. Fast Free-Carrier Diffusion in $CH_3NH_3PbBr_3$ Single Crystals Revealed by Time-Resolved One- and Two-Photon Excitation Photoluminescence Spectroscopy. *Adv. Electron. Mater.* **2016**, *2*, 1500290.

(17) Pazos-Outón, L. M.; Szumilo, M.; Lamboll, R.; Richter, J. M.; Crespo-Quesada, M.; Abdi-Jalebi, M.; Beeson, H. J.; Vrućinić, M.; Alsari, M.; Snaith, H. J.; Ehrler, B.; Friend, R. H.; Deschler, F. Photon Recycling in Lead Iodide Perovskite Solar Cells. *Science* **2016**, *351*, 1430-1433.

(18) Kirchartz, T.; Staub, F.; Rau, U. Impact of Photon Recycling on the Open-Circuit Voltage of Metal Halide Perovskite Solar Cells. *ACS Energy Lett.* **2016**, *1*, 731-739.

(19) Yamada, T.; Yamada, Y.; Nakaike, Y.; Wakamiya, A.; Kanemitsu, Y. Photon Emission and Reabsorption Processes in $CH_3NH_3PbBr_3$ Single Crystals revealed by Time-Resolved Two-Photon-Excitation Photoluminescence Microscopy. *Phys. Rev. Appl.* **2017**, *7*, 014001.

(20) Yamada, T.; Aharen, T.; Kanemitsu, Y. Near-Band-Edge Optical Responses of $CH_3NH_3PbCl_3$ Single Crystals: Photon Recycling of Excitonic Luminescence. *Phys. Rev. Lett.* **2018**, *120*, 057404.

(21) Dursun, I.; Zheng, Y.; Guo, T.; De Bastiani, M.; Turedi, B.; Sinatra, L.; Haque, M. A.; Sun, B.; Zhumekenov, A. A.; Saidaminov, M. I.; de Arquer, F. P. G.; Sargent, E. H.; Wu, T.; Gartstein, Y. N.; Bakr, O. M.; Mohammed, O. F.; Malko, A. V. Efficient

Photon Recycling and Radiation Trapping in Cesium Lead Halide Perovskite Waveguides. *ACS Energy Lett.* **2018**, *3*, 1492-1498.

(22) Gan, Z.; Wen, X.; Chen, W.; Zhou, C.; Yang, S.; Cao, G.; Ghiggino, K. P.; Zhang, H.; Jia, B. The Dominant Energy Transport Pathway in Halide Perovskites: Photon Recycling or Carrier Diffusion? *Adv. Energy Mater.* **2019**, *9*, 1900185.

(23) Fang, Y.; Wei, H.; Dong, Q.; Huang, J. Quantification of Re-absorption and Re-emission Processes to Determine Photon Recycling Efficiency in Perovskite Single Crystals. *Nat. Commun.* **2017**, *8*, 14417

(24) Davis, N. J. L. K.; de la Peña, F. J.; Tabachnyk, M.; Richter, J. M.; Lamboll, R. D.; Booker, E. P.; Rivarola, F. W. R.; Griffiths, J. T.; Ducati, C.; Menke, S. M.; Deschler, F.; Greenham, N. C. Photon Reabsorption in Mixed $CsPbCl_3$:$CsPbI_3$ Perovskite Nanocrystal Films for Light-Emitting Diodes. *J. Phys. Chem. C* **2017**, *121*, 3790-3796.

(25) Bouduban, M. E. F.; Burgos-Caminal, A.; Ossola, R.; Teuschera, J.; Moser, J.-E. Energy and Charge Transfer Cascade in Methylammonium Lead Bromide Perovskite Nanoparticle Aggregates. *Chem. Sci.* **2017**, *8*, 4371-4380.

(26) de Weerd, C.; Gomez, L.; Zhang, H.; Buma, W. J.; Nedelcu, G.; Kovalenko, M. V.; Gregorkiewicz, T. Energy Transfer between Inorganic Perovskite Nanocrystals. *J. Phys. Chem. C* **2016**, *120*, 13310-13315.

(27) Ghimire, S.; Nair, V. C.; Muthu, C.; Yuyama, K.; Vacha, M.; Biju, V. Photoinduced Photoluminescence Enhancement in Self-Assembled Clusters of Formamidinium Lead Bromide Perovskite Nanocrystals. *Nanoscale* **2019**, *11*, 9335-9340.

(28) Aristidou, N.; Sanchez-Molina, I.; Chotchuangchutchaval, T.; Brown, M.; Martinez, L.; Rath, T.; Haque, S. A. The Role of Oxygen in the Degradation of Methylammonium Lead Trihalide Perovskite Photoactive Layers. *Angew. Chem. Int. Ed.* **2015**, *54*, 8208-8212.

(29) Yang, J.; Yuan, Z.; Liu, X.; Braun, S.; Li, Y.; Tang, J.; Gao, F.; Duan, C.; Fahlman, M.; Bao, Q. Oxygen- and Water-Induced Energetics Degradation in Organometal Halide Perovskites. *ACS Appl. Mater. Interfaces* **2018**, *10*, 16225-16230.

(30) Jodlowski, A. D.; Yépez, A.; Luque, R.; Camocho, L.; de Miguel, G. Benign-by-Design Solventless Mechanochemical Synthesis of Three-, Two-, and One-Dimensional Hybrid Perovskites. *Angew. Chem. Int. Ed.* **2016**, *55*, 14972-14977.

(31) Jana, A.; Mittal, M.; Singla, A.; Sapra, S. Solvent-Free, Mechanochemical Syntheses of Bulk Trihalide Perovskites and their Nanoparticles. *Chem. Comm.* **2017**, *53*, 3046-3049.

(32) Prochowicz, D.; Yadav, P.; Saliba, M.; Saski, M.; Zakeeruddin, S. M.; Lewiński, J.; Grätzel, M. Mechanosynthesis of Pure Phase Mixed-Cation $MA_xFA_{1-x}PbI_3$ Hybrid Perovskites: Photovoltaic Performance and Electrochemical Properties. *Sustainable Energy Fuels* **2017**, *1*, 689-693.

(33) Askar, A. M.; Karmakar, A.; Bernard, G. M.; Ha, M.; Terskikh, V. V.; Wiltshire, B. D.; Patel, S.; Fleet, J.; Shankar, K.; Michaelis, V. K. Composition-Tunable Formamidinium Lead Mixed Halide Perovskites via Solvent-Free Mechanochemical Synthesis: Decoding the Pb Environments using Solid-State NMR Spectroscopy. *J. Phys. Chem. Lett.* **2018**, *9*, 2671-2677.

(34) Hirose, K.; Sinmyo, R.; Hernlund, J. Perovskite in Earth's Deep Interior. *Science* **2017**, *358*, 734-738.

(35) Wang, Y.; Lü, X.; Yang, W.; Wen, T.; Yang, L.; Ren, X.; Wang, L.; Lin, Z.; Zhao, Y. Pressure-Induced Phase Transformation, Reversible Amorphization, and Anomalous Visible Light Response in Organolead Bromide Perovskite. *J. Am. Chem. Soc.* **2015**, *137*, 11144-11149.

(36) Jaffe, A.; Lin, Y.; Beavers, C. M.; Voss, J.; Mao, W. L.; Karunadasa, H. I. High-Pressure Single-Crystal Structures of 3D Lead-Halide Hybrid Perovskites and Pressure Effects on their Electronic and Optical Properties. *ACS Cent. Sci.* **2016**, *2*, 201-209.

(37) Cao, Y.; Qi, G.; Liu, C.; Wang, L.; Ma, Z.; Wang, K.; Du, F.; Xiao, G.; Zou, B. Pressure-Tailored Band Gap Engineering and Structure Evolution of Cubic Cesium Lead Iodide Perovskite Nanocrystals. *J. Phys. Chem. C* **2018**, *122*, 9332-9338.

(38) Baikie, T.; Barrow, N. S.; Fang, Y.; Keenan, P. J.; Slater, P. R.; Piltz, R. O.; Gutmann, M.; Mhaisalkar, S. G.; White, T. J. A Combined Single Crystal Neutron/X-Ray Diffraction and Solid-State Nuclear Magnetic Resonance Study of the Hybrid Perovskites $CH_3NH_3PbX_3$ (X = I, Br and Cl). *J. Mater. Chem. A* **2015**, *3*, 9298-9307.

(39) Yang, M.; Peng, H.-S.; Zeng, F.-L.; Teng, F.; Qu, Z.; Yang, D.; Wang, Y.-Q.; Chen, G.-X.; Wang, D.-W. In Situ Silica Coating-Directed Synthesis of Orthorhombic Methylammonium Lead Bromide Perovskite Quantum Dots with High Stability. *J. Colloid Interface Sci.* **2018**, *509*, 32-38.

(40) Wang, K.-H.; Li, L.-C.; Shellaiah, M.; *J. Mater. Chem. A* **2015**, *3*, 9298-9307. Structural and Photophysical Properties of Methylammonium Lead Tribromide ($MAPbBr_3$) Single Crystals. *Sci. Rep.* **2017**, *7*,13643.

(41) Galkowski, K.; Mitioglu, A.; Miyata, A.; Plochocka, P.; Portugall, O.; Eperon, G. E.; Wang, J. T.-W.; Stergiopoulos, T.; Stranks, S. D.; Snaith, H. J.; Nicholas, R. J. Determination of the Exciton Binding Energy and Effective Masses for Methylammonium and Formamidinium Lead Tri-Halide Perovskite Semiconductors. *Energy Environ. Sci.* **2016**, *9*, 962-970.

(42) Chin, X.Y.; Cortecchia, D.; Yin, J.; Bruno, A.; Soci, C. Lead Iodide Perovskite Light-Emitting Field-Effect Transistor. *Nat. Commun.* **2015**, *6*, 7383.

(43) Manser, J. S.; Christians, J. A.; Kamat, P. V. Intriguing Optoelectronic Properties of Metal Halide Perovskites. *Chem. Rev.* **2016**, *116*, 12956-13008.

(44) Tanaka, K.; Takahashi, T.; Ban, T.; Kondo, T.; Uchida, K.; Miura, N. Comparative Study on the Excitons in Lead-Halide-Based Perovskite-Type Crystals $CH_3NH_3PbBr_3$ $CH_3NH_3PbI_3$. *Solid State Commun.* **2003**, *127*, 619-623.

(45) Even, J.; Pedesseau, L.; Jancu, J.-M.; Katan, C. Importance of Spin–Orbit Coupling in Hybrid Organic/Inorganic Perovskites for Photovoltaic Applications. *J. Phys. Chem. Lett.* **2013**, *4*, 2999-3005.

(46) Even, J.; Pedesseau, L.; Katan, C. Analysis of Multivalley and Multibandgap Absorption and Enhancement of Free Carriers Related to Exciton Screening in Hybrid Perovskites. *J. Phys. Chem. C* **2014**, *118*, 11566-11572.

TOC Graphic

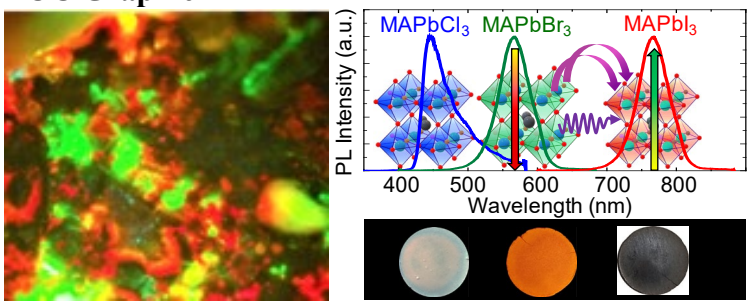
MAPbCl3
MAPbBr3
MAPbI3
PL Intensity (a.u.)
400
500
600
700
800
Wavelength (nm)